Enhanced visualization of the retinal vasculature using depth information in OCT

Joaquim de Moura · Jorge Novo · Pablo Charlón · Noelia Barreira · Marcos Ortega

Abstract Retinal vessel tree extraction is a crucial step for analyzing the microcirculation, a frequently needed process in the study of relevant diseases. To date this has normally been done by using 2D image capture paradigms, offering a restricted visualization of the real layout of the retinal vasculature.

In this work, we propose a new approach that automatically segments and reconstructs the 3D retinal vessel tree by combining near-infrared reflectance retinography information with Optical Coherence Tomography (OCT) sections. Our proposal identifies the vessels, estimates their calibers and obtains the depth at all the positions of the entire vessel tree, thereby enabling the reconstruction of the 3D layout of the complete arteriovenous tree for subsequent analysis.

The method was tested using 991 OCT images combined with their corresponding near-infrared reflectance retinography. The different stages of the methodology were validated using the opinion of an expert as a reference. The tests offered accurate results, showing coherent reconstructions of the 3D vasculature that can be analyzed in the diagnosis of relevant diseases affecting the retinal microcirculation, such as hypertension or diabetes, among others.

Keywords Computer-aided diagnosis · vascular structure · retinal imaging · Optical Coherence Tomography

J. de Moura, J. Novo, N. Barreira, M. Ortega
Dep. Computación, Universidade da Coruña, 15071 A Coruña, Spain
Tel.: +34-881011330
Fax: +34-981167160
E-mail: joaquim.demoura@udc.es,jnovo@udc.es,nbarreira@udc.es,mortega@udc.es

P. Charlón
Instituto Oftalmológico Victoria de Rojas, A Coruña, Spain E-mail: pcharlon@sgoc.es

1 Introduction

The analysis of the retina is frequently used in many relevant diagnostic procedures as useful information can be obtained for diseases such as hypertension or diabetes. Computer-aided diagnosis (CAD) systems can thus be of the utmost importance in assisting clinicians in the different diagnostic processes, facilitating and simplifying their work.

The retinal vessel tree is one of the most widely examined structures as it represents the most direct and least invasive way to observe the human circulatory system. Hence, analysis of the retinal vasculature has proved extremely useful due to its relation with a number of pathologies. In this regard, some works have stated that retinal vasculature calibers are a significant biomarker for diabetes [16,23]. Smith *et al.* [29] also identified retinal vasculature caliber as a relevant sign in the analysis of hypertension as small vessel changes can anticipate the presence of severe hypertension. Other studies [26,7] have also defined calculations on the microcirculation of the retina as possible indices for cerebrovascular disease as well as for other cardiovascular illness events related to retinal vasculature calibers [32,35]. The retinal vasculature has also demonstrated its usefulness in other problems as is the case, for example, in biometrics, where vessel intersections are used in a similar manner to fingerprints [25].

The most widely-used image modalities in this respect are angiography and retinography, which give a 2D representation of the real layout of the eye fundus. Most of the proposals in the literature were made using these image modalities, providing only a partial representation of the vessel tree. Some surveys have described the various proposals that have been put forward in the matter [12], and representative examples of the principal paradigms employed will now be described.

Thresholding is one of the methodologies used in the problem, as in the works of Zhang *et al.* [43] or Yong *et al.* [42] where adaptive thresholds were designed in processes that aimed for the localization and segmentation of the vessels. Xiaoyi and Mojon [38] designed a sophisticated framework that includes adaptive local thresholding in an approach combining hypothetical thresholds and a posterior verification step.

Tracking approaches have also been implemented, as in the work of Wink *et al.* [34], who designed a semi-automatic method that starts from a set of user-defined points in the image and retrieves the central axis of tubular structures. For that purpose, a vectorial multiscale feature image was included for wave front propagation, a process that adapts perfectly to the problem of multiscale vessels. Mendonça and Campilho [21] presented a methodology that combines the extraction of the centerline of the vasculature with the subsequent application of region growing to construct the final vessel segmentation. Lazar and Hajdu [18] implemented a region growing process that integrates a hysteresis thresholding scheme including the response vector similarity of adjacent pixels.

Different edge detector approaches have also been used to deal with the issue, including specific improvements since they normally present certain draw-

backs in the detection of vessels in noisy scenes or blurred contours. Dhar *et al.* [8] studied the robustness of the Canny and Laplacian of Gaussian detectors, demonstrating that the Canny filter offers a more stable behavior in a variety of image conditions. Xiaolin *et al.* [37] modified Canny with a bilateral filter to remove noisy artifacts and facilitate vessel detection.

As in many other medical imaging procedures, Wavelet transform has shown its potential in this particular application, as demonstrated in the proposal by Fathi *et al.* [10], which provided satisfactory results integrating the information over multiple classification scales. Nayak *et al.* [22] also employed the Wavelet transform for the purpose of vessel identification in a context of patients that presented diabetic retinopathy. Soares *et al.* [30] designed a methodology that used a 2D Gabor Wavelet over multiple scales as the feature for a classification process with a Bayesian classifier.

Chen *et al.* [4] used graph-cuts in an unsupervised approach to identify the vessels, as did Xu *et al.* [40], where vessel width is derived in a segmentation process using a graph-theoretic method.

Of all the strategies employed, Artificial Neural Networks (ANNs) is one of the most widely referenced in many different medical imaging procedures, as they usually provide correct results in largely complex problems. ANNs appear frequently in the ophthalmological research field, as in the work by Sinthanayothin *et al.* [28], where neural networks extract the main structures of the eye fundus such as the optic disc, the fovea or the blood vessels. Li *et al.* [19] approached the problem as a modality data transform, using a neural network that discriminates vessel pixels in the image. In the work of Alonso-Montes *et al.* [1], the proposed method included a Convolutional Neural Network (CNN) with the aim of optimizing vascular tree extraction in order to meet real-time requirements. Jiang *et al.* [15] used ANNs characterizing the pixels with a 8-D vector composed of intensity descriptors and pixel strength features and subsequently trained the network to achieve the segmentation. Vega *et al.* [33] developed an elaborate network they refer to as a Lattice Neural Network with Dendritic Processing (LNNDP) to extract the vessels with successful results. Other classifiers were also considered, such as random forest in the work by Cheng *et al.* [5], where the authors defined a large and heterogeneous set of features combined with the above-mentioned classifier.

Approaches that exploit different kinds of pattern analysis have also appeared in the literature. Staal *et al.* [31] searched for ridges to detect the lines which match with vessel centerlines. The line elements are then partitioned in patches to extract features and perform the final vessel detection using a K-NN classifier. Kovacs and Hajdu [17] designed a process of template matching using generalized Gabor function-based templates to detect the centerlines and subsequently applying a reconstruction step to obtain the final segmentation. Chakraborti *et al.* [3] implemented a self-adaptive matched filter combining vesselness filtering with a high degree of sensitivity for the detection of vessels in retinographies. Yin *et al.* [41] constructed an orientation aware-detector based on the principle that the vessels are locally oriented and have linearly elongated structures. Imani *et al.* [14] used a morphological component analy-

sis (MCA) algorithm in a method that overcomes the difficulties of the problem in retinographies with lesions, facilitating the discrimination between vessels and lesions.

More recently, Optical Coherence Tomography Angiography (OCTA) has emerged as an image modality that uses the spectral domain for a non-invasive visualization of the retinal and choroidal vasculature [6]. The use of OCTA is not yet widespread in health services due to its recent appearance and the high cost of acquiring this type of technology.

Optical Coherence Tomography (OCT) imaging is widely used in clinical services. It offers additional depth information instead of the classical 2D layouts provided by angiographies and retinographies. This information is crucial for obtaining the real 3D layout of the retinal vessels and enabling clinicians to perform an analysis that comes closer to reality. Only a small number of works have appeared that use OCT images to deal with the issue of vasculature segmentation. Moreover, these few proposals consist of limited methodologies that still offer 2D representations of the retinal vasculature. In this regard, Niemeijer *et al.* [24] presented an approach that segments the retina in multiple layers with the vessel projections and performs a classification stage in the projected image to extract the vessels. Xu *et al.* [39] implemented a 3D boosting learning to detect the vessels, after which the method applies a post-processing to remove false positive detections. In the work of Pilch *et al.* [27] statistical shape models were considered with manually segmented vessels. This vessel set was then used for a subsequent training stage. Once trained, the resulting model is used to identify the final contours of the vessels in the axial direction. Guimaraes *et al.* [13], in a study of abnormal retinal vascular patterns, identified the vessel depths at all the positions using the OCT images. In the work of Wu *et al.* [36] Coherent Point Drift was included in an approach for the segmentation of the vessel points. These points are established as landmarks in a context of image registration.

In such a context, this work presents a complete methodology for 3D extraction of the retinal vessel tree and its 3D reconstruction using OCT images. Hence, a more complete vasculature representation permits a more reliable analysis of the retinal microcirculation that is needed in many diagnostic processes.

This paper is organized as follows. Section 2 presents the proposed methodology and the characteristics of all the stages. Section 3 presents some practical results and the validation of key steps of the proposal, compared to the manual annotations of a clinician. Finally, Sections 4 and 5 include the discussion and conclusions of this proposal as well as possible future work.

2 Methods

The proposed method receives, as input, a set of OCT images. The images correspond to consecutive OCT sections that represents the morphology of the retinal layers. This technique provides tomographic images of the biologi-

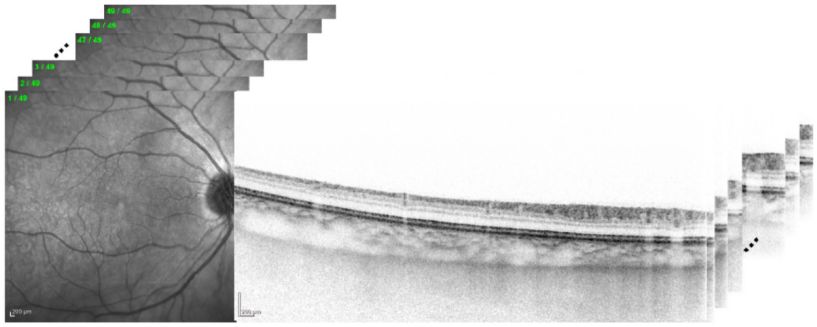

Fig. 1 Set of OCT sections in combination with the near-infrared reflectance retinography.

cal tissue with high resolution in progressive scans over the eye fundus of the patient. These images are complemented with the corresponding near-infrared reflectance retinography that is provided in combination with the OCT sections. Both sources of information, the consecutive OCT sections and the corresponding near-infrared retinography, are directly provided by the capture machine. Figure 1 illustrates an OCT scan composed of the near-infrared reflectance retinography and the consecutive OCT sections.

The method is organized in a set of progressive stages. Firstly, the arteriovenous tree is extracted in the near-infrared reflectance retinography, constructing the set of segments that represents the vessels and correcting all the detected misrepresentations at the intersections. Subsequently, diameters over the detected points are calculated. The vessel segments are then mapped in the input OCT sections with the aim of identifying the depth, z, coordinates. The 3D segmentation is finally constructed with the obtained coordinates. For this purpose an interpolation using splines of the extracted vasculature is calculated to provide a smooth representation. Figure 2 describes the general scheme of the proposed methodology, each stage of which will be detailed in the following subsections.

2.1 2D vessel extraction

The vessels are initially segmented in the near-infrared reflectance retinography to obtain the first (x, y) coordinates, given its simplicity and well-established techniques. We used an approach that involves different morphological operators [2] to obtain an initial representation of the vessels. The segmentation process is performed in two main stages: vascular structure enhancement and extraction of the arteriovenous tree.

Firstly, a top-hat filter [9] is used to enhance the biggest and darkest structures in the image, corresponding to the vessels. Then, the noise and vascular

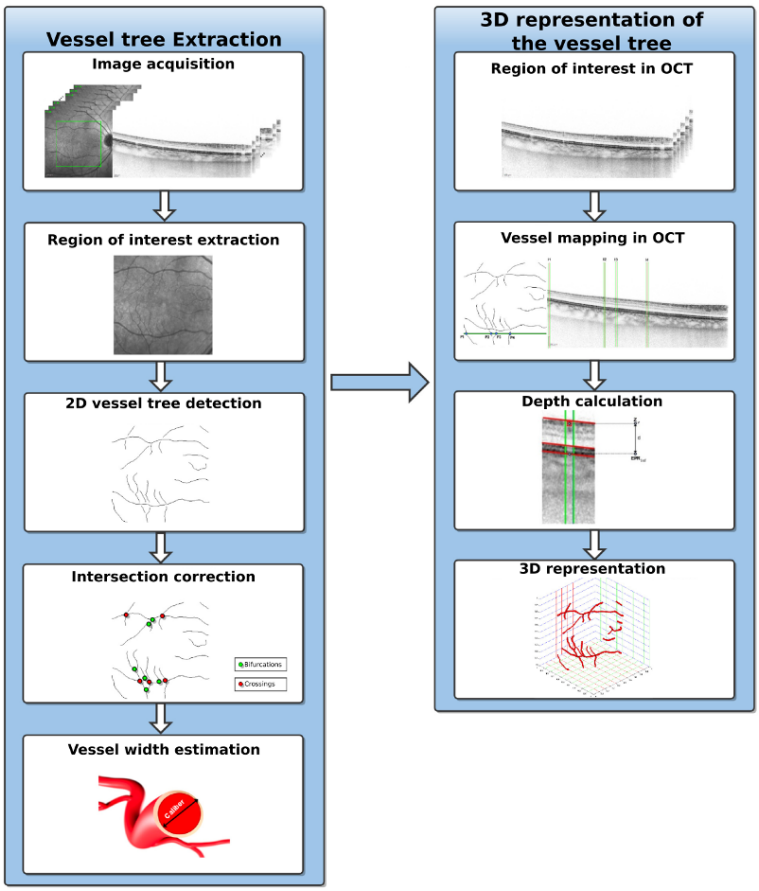

Fig. 2 Scheme of the proposed methodology.

reflex is minimized with a median filter, thus facilitating the extraction of a more precise segmentation.

Vessel enhancement is done using the eigenvalues, λ_1 and λ_2, of the Hessian matrix [11], these being combined to enhance tubular structures of variable size and therefore identify vessels at different scales. Thus, a function $B(p)$ is formulated as:

$$B(p) = \begin{cases} 0 & \lambda_2 > 0 \\ exp(\frac{-R_B^2}{2\beta^2})(1 - exp(-\frac{S^2}{2c^2})) & otherwise \end{cases} \quad (1)$$

where $R_B = \lambda_1/\lambda_2$, c is half of the max Hessian norm and S measures the "second order structures". Pixels that belong to vessels are normally represented by small λ_1 values and higher positive λ_2 values. This way, we reinforce

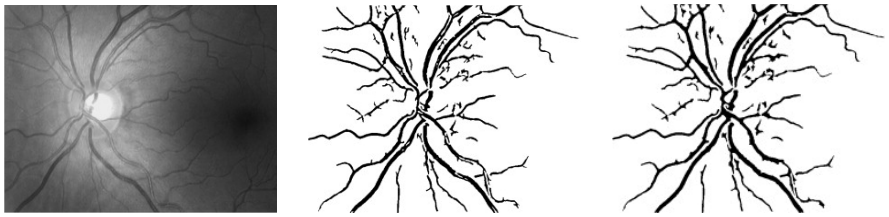

(a) (b) (c)

Fig. 3 Segmentation process of the vessel tree. (a) Original image. (b) Result after preprocessing, enhancement, hysteresis thresholding and cleaning of small structures. (c) Final result after dilation step.

the robustness of the method by minimizing the influence of the input image characteristics in the parameters of the system.

After this enhancement, vascular segmentation is achieved in two steps: an initial segmentation and the subsequent removal of isolated structures. The initial segmentation is done by means of a hysteresis-based thresholding. A hard threshold (T_h) obtains pixels with a high confidence of being vessels while a weak threshold (T_w) keeps all the pixels of the tree, including the spurious ones. The final vessel segmentation is formed by all the pixels included by T_w that are connected to at least one pixel obtained by T_h. The values for T_h and T_w are calculated from two image properties: the percentage of image representing vessels and the percentage of image representing fundus. The gap between both percentages will include all the non- classified pixels. The values for the thresholds are easily derived after calculating the percentiles with:

$$P_k = L_k + \frac{k(n/100) - F_k}{f_k} \times c, \quad k = 1, 2, ..., 99 \tag{2}$$

where $L - k$ is percentile lower limit k, n indicates the size of the set, F_k is the accumulated frequency for $k - 1$, f_k measures the frequency of percentile k and c is the size of the percentile interval (1 in this case).

As the images can include noisy artifacts due to capture devices or pathologies, a cleaning step is then applied. All isolated detections smaller than a given size are removed from the results. Finally, as this strategy can produce discontinuity inside the vessels, a final dilation process is applied with the result that vessel borders grow towards the centre, filling the existing gaps. This dilation process is done using a modified median filter. In order to avoid an erosion when the filter is applied to the external border of the vessels, the resulting value will only be set if it is a vessel pixel. To "fill" as many white gaps as possible the dilation process is applied iteratively, repeated N times to guarantee the filling of the vessels. Figure 3 illustrates this vessel segmentation approach with an example.

2D segmentation methodologies typically present cumulative errors as they misrepresent the edges of the vessels. For that reason, their direct use for vasculature reconstruction is not recommended. Instead, proposals that identify

the centerline of the vessels are desired to correct possible deviations in the detections. Firstly, our proposal identifies the vessels as a set of segments that identify the approximate centerlines. We used the strategy explained in [25] where curvature level curves are used to identify the creases (crest and valley lines) that identify the vessels. In particular, Level Set Extrinsic Curvature (LSEC) was implemented in this work, Eq. 3, given its invariant properties. The result of this method identifies the entire centerline of the vessels, a kernel structure that is subsequently used in the 3D vessel reconstruction. Given a function $L : \mathbb{R}^d \rightarrow \mathbb{R}$, the level set for a constant l consists of the set of points $x|L(x) = l$. For 2D images, L can be considered as a topographic relief or landscape and the level sets as its level curves. Negative minima of the level curve curvature k, level by level, form valley-like curves and positive maxima ridge-like curves.

$$k = (2L_xL_yL_{xy} - L_y^2L_{xx} - L_x^2L_{yy})(L_x^2 + L_y^2)^{-\frac{3}{2}} \tag{3}$$

where

$$L_\alpha = \frac{\partial L}{\partial \alpha}, L_{\alpha\beta} = \frac{\partial^2 L}{\partial \alpha\, \partial \beta}, \alpha, \beta \in x, y \tag{4}$$

However, the usual discretization of LSEC is ill-defined in a number of cases, giving rise to unexpected discontinuities at the centre of elongated objects. Due to this, the Multilocal Level Set Extrinsic Curvature with Structure Tensor, MLSEC-ST operator, originally defined [20] for 3D landmark extraction of CT and MRI volumes, is used:

$$k = -div(\bar{w}) = -\sum_{i=1}^{d}(\frac{\partial \bar{w}^i}{\partial x^i}), d = 2; \tag{5}$$

where $\bar{w}^i$ is the component at the position i of $\bar{w}$, the normalized vector field of $L : \mathbb{R}^d \rightarrow \mathbb{R}$. This last is defined by Eq. 6, where O_d is the d-dimensional zero vector.

$$\bar{w} = \begin{cases} \frac{w}{\|w\|}, \; if \; \|w\| > 0 \\ O_d, \; if \; \|w\| = 0 \end{cases} \tag{6}$$

Although the method finds the approximate centerline, it detects more than 1-pixel width vessel segmentations as the vessels present different degrees of creaseness over their structure. All the detected pixels are subsequently assigned to a particular segment to guarantee that all of them only belong to a single one. In this way we obtain a skeletonized vessel tree, organized by a set of segments that are represented by two end points and a list of consecutive pixels. Finally, small segments are filtered from the results considering that these detections belongs to other noisy structures that can appear in the eye fundus, as shown in Figures 4,(a),(b) and (c).

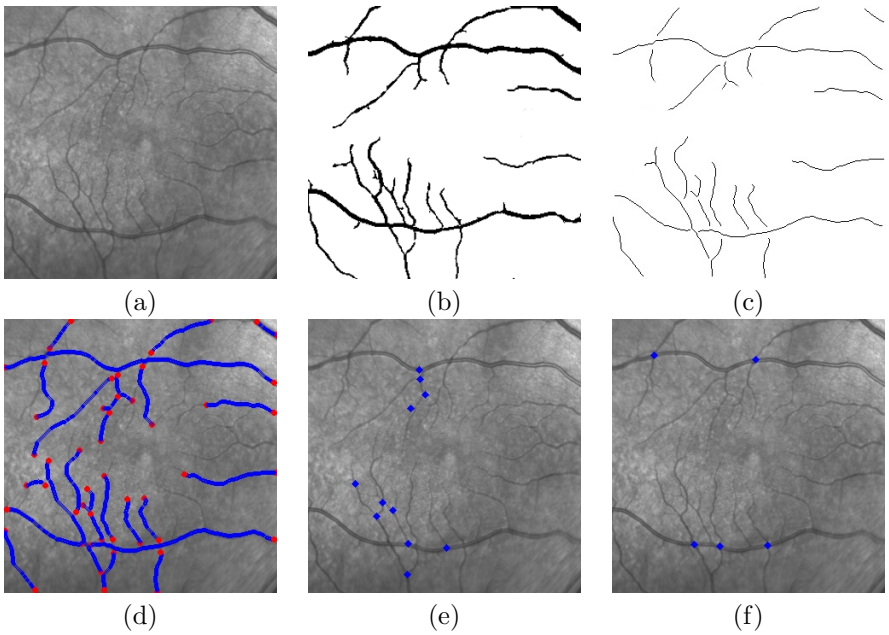

Fig. 4 2D vessel tree extraction process. (a) Input retinography. (b) 2D Vessel tree segmentation. (c) Skeletonized segments. (d) Detected end points. (e) Bifurcations to be corrected. (f) Crossings to be corrected.

2.2 Intersections correction

The crease procedure presents a significant limitation due to the many problems it experiences in correctly identifying vessels at intersections. This occurs because the method is unable to identify the crease directions in these areas, as shown in (Figure 4, d). All these intersections are revised to correct any wrong detection. The main objective consists of recovering, by joining segments, the information lost in the crease extraction phase. Hence, all detected end points are categorized as either belonging to a bifurcation, belonging to a crossing or being correctly identified as an end.

- **Bifurcations**. For each end point the closest distance to any other segment is calculated and those under a given threshold are marked for joining in a bifurcation of a single vessel. The identified end point is connected to this closest segment by interpolation using its own continuity. Figure 5 illustrates the situation with an example of a bifurcation and the correction that was performed in the intersection.
- **Crossings**. Two end points that are significantly close to a crossing segment. When a pair of end points is within a given threshold, the continuity between them is considered. In this case, the points are connected by in-

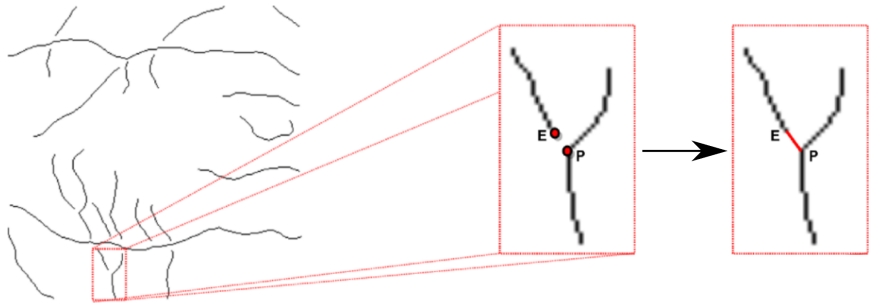

Fig. 5 Example of a detected bifurcation and the corresponding correction made.

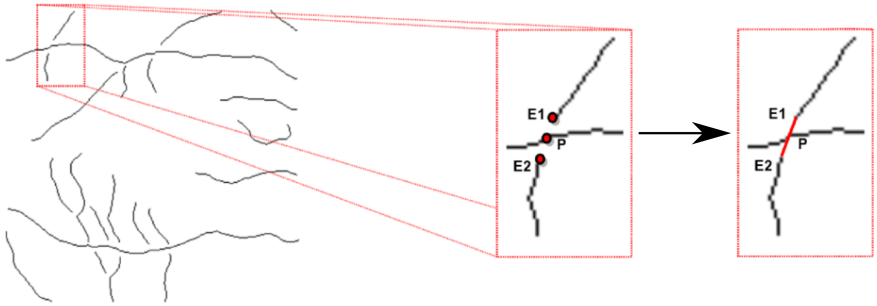

Fig. 6 Example of a detected crossing and the corresponding correction made.

terpolation and belong, as a result, to a single segment. Figure 6 presents an example of crossing and the corresponding correction.

The end points that are neither marked as bifurcations nor crossings are directly considered as correctly detected end points. Figures 4,(d),(e) and (f) show an example of the process of analysis and correction of end points.

2.3 Caliber estimation

In addition to vessel coordinates, we also need to determine their calibers for the 3D reconstruction. The orientation of a vessel at a coordinate, θ, is calculated as the angle between consecutive vessel points $P_1(x_1, y_1)$ and $P_2(x_2, y_2)$ as:

$$\theta = arctan\left(\frac{y_2 - y_1}{x_2 - x_1}\right) \tag{7}$$

The caliber is then estimated in the perpendicular directions of θ, as Figure 7(a) illustrates. We analyze the initial vessel segmentation image was previously obtained by the crease method to find the width at each point. Hence,

(a) (b)

Fig. 7 Diameter estimation. (a) Representation of the analyzed direction at each point of a segment. (b) Example of a segment overlapping the vessel.

the method looks for the edges (limits of the vessel) in each perpendicular direction, an easy process in a binary image. Finally, two distances, r_1 and r_2, are calculated as the distance from the centerline to the edges. Their sum indicates the final caliber at the point in question:

$$d = r_1 + r_2 \tag{8}$$

Vessel caliber is searched in both directions as the detected centerlines are not always exactly placed in the center of the vessels, as is the case of the example shown in Figure 7(b). Therefore, the sum of both distances produces a more accurate estimation of a vessel's caliber.

2.4 Mapping in the OCT images

The depth position of the vessels, z, is calculated using the depth information that is provided in the OCT sections.

In the OCT images, any structures that appear in the eye fundus, in our case vessels, block the transmission of light and therefore leave a shadow proportional to their size. Figure 8 includes an OCT image where the shadows of several vessels are delimited.

Each OCT section corresponds to a band in the 2D retinography. The positions of the vessels in the OCT sections are represented by the intersections of the band and the vessel tree in the 2D retinography. These intersections identify the columns of the band where the vessels are located, and are mapped in their corresponding OCT sections. A search is made for intersections in the retinography in all the bands that correspond to the OCT sections, making it possible to identify all the columns of the OCT sections in which vessels are to be be found. This process is repeated for all the bands in the 2D retinography that correspond with the OCT sections. Then, a rectangle with the same size as the calculated caliber is constructed, $r_1 + r_2$, that matches with the projection zone, or in other words with the shadow produced by the vessel. This process is illustrated in Figure 9.

This projection zone, delimited by the constructed rectangle, contains the vessel location. By identifying its position we can derive the corresponding

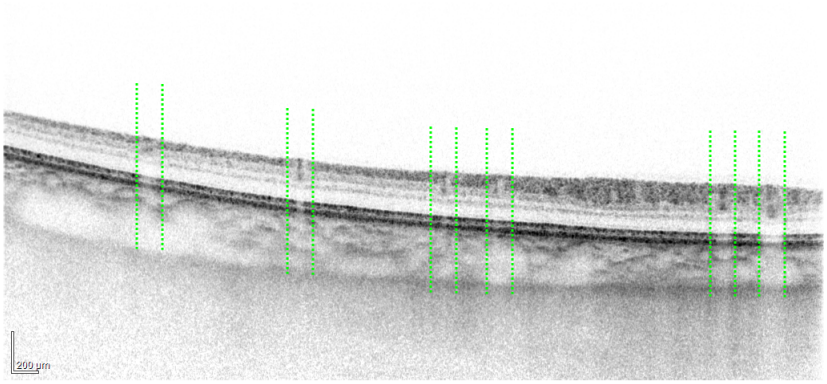

Fig. 8 Example of the shadow projection caused by a set of vessels.

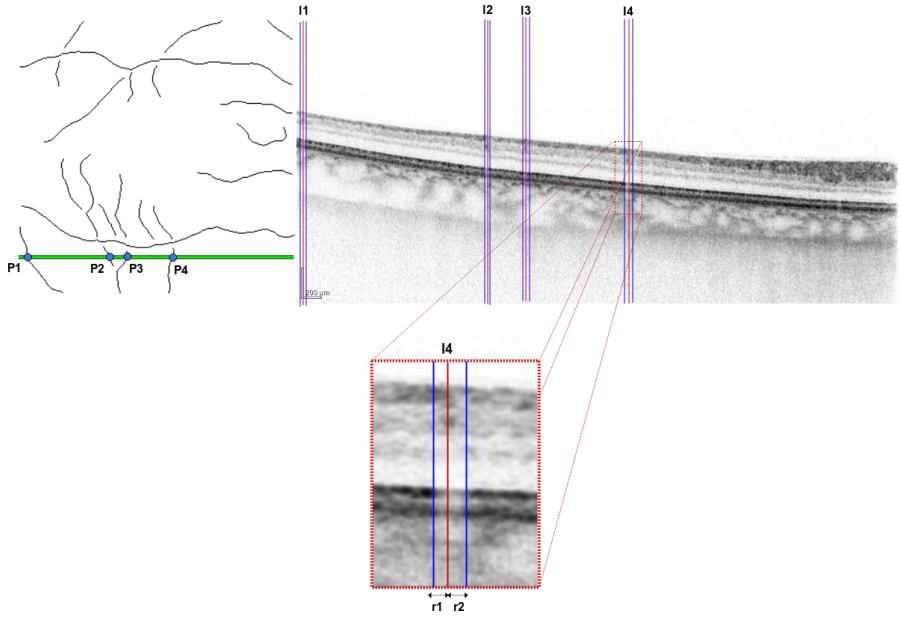

Fig. 9 Mapping process of vessel coordinates in OCT. Identification of the projection zone.

depth z of the vessel coordinate. Figure 10 includes the location of a vessel inside the projection zone of the OCT section.

2.5 Vessel depth estimation

The method calculates the depths, z, in 3 progressive stages:

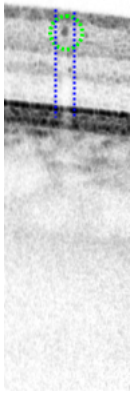

Fig. 10 Vessel location inside its projection zone in a OCT band.

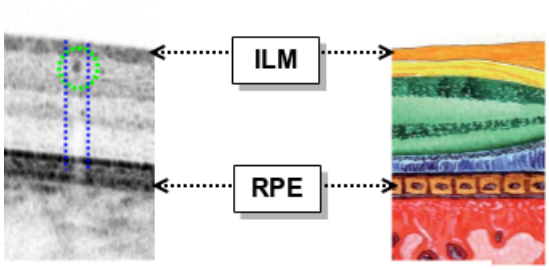

Fig. 11 ILM and RPE layers inside the section of an OCT image.

Identification of the ILM and RPE layers. Inside the projection zone, we can restrict the search region to the retinal layers that delimit the possible vessel location. This search space is enclosed by the Inner Limiting Membrane (ILM) and the Retinal Pigment Epithelium (RPE) retinal layers. Figure 11 identifies the ILM and RPE inside an OCT section of an OCT image.

Firstly, a Gaussian filtering is applied to smooth the image and remove noise. As both ILM and RPE show the edges with the largest contrast of all the layers, Canny edge detector is then applied to find these limits. A horizontal gradient is used to obtain the strongest and clearest detections of both layers. As a result, the upper and lower connected lines delimit both ILM and RPE layers. Figure 12 includes the results of the detection of both layers.

Vessel location. The vessels appear in the OCT images as dark elliptic areas. Therefore, we search for the darkest neighborhood between ILM and

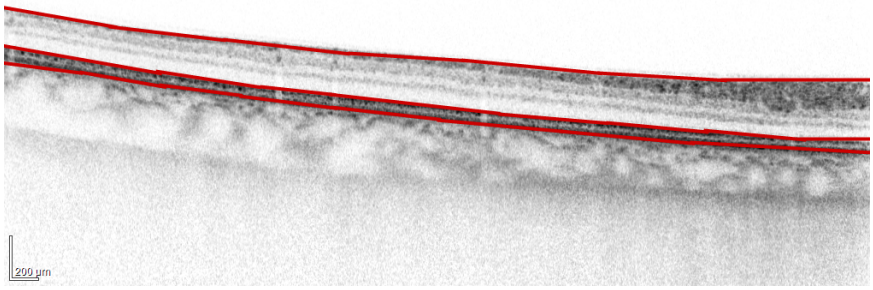

Fig. 12 Identification process of the ILM and RPE layers in a OCT section.

Fig. 13 Vessel detection in an OCT section inside the search region between ILM and RPE layers.

RPE layers. The darkest point of the darkest neighborhood is marked as the vessel center (Figure 13). To reinforce the detection, a mean filter of 3×3 size is previously used to remove possible noisy dark pixels and minimize the risk of wrong detections.

Final depth estimation. Finally, the depth coordinate z is derived using the RPE layer as baseline and calculating the distance from it to the detected location of the vessel:

$$z = |C_v - P_i| \tag{9}$$

where C_v measures the the vessel location in the OCT section and P_i the baseline of the RPE layer.

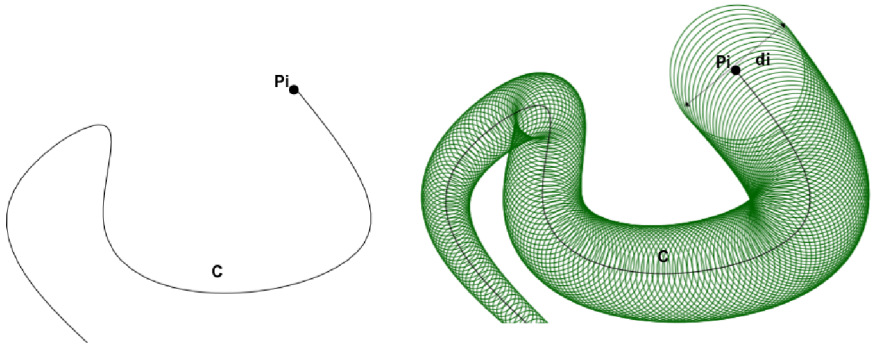

Fig. 14 Representation of a 3D tubular structure associated to a curve.

2.6 3D vasculature reconstruction

The vessels are represented by segments S, where each point P_i of a segment S is represented by the 3D coordinates (x, y, z) and its diameter d, parameters that were previously calculated. Interpolation by splines is used with the entire set of points of S connecting them in a curve. This permits a smooth representation to be visualized, minimizing abrupt transitions between vessel coordinates of consecutive OCT sections in images with low OCT image resolution.

The vasculature is reconstructed as tubular shapes (due to the tubular structure of the vessels) centering on the centerline points P_i with a diameter size equivalent to the calibers, d. Figure 14 illustrates this 3D representation process over a curve.

3 Results

The proposed method was validated with an image dataset of 991 OCT sections from 21 patient scans. The local ethics committee approved the study and the tenets of the Declaration of Helsinki were followed. These images were captured with a Spectralis® OCT confocal scanning laser ophtalmoscope from Heidelberg Engineering. The image acquisition was done by selecting the dense volume scan type over a scan angle of ($20° \times 20°$, roughly $6mm \times 6mm$) consisting of 49 B-mode scans acquired utilizing Automatic Real-Time (ART Mean) = 16 (number of scans averaged). B-mode scans are separated by $120\mu m$ between each other and composed of 1024 A-mode scans, with a separation of $5.5\mu m$. Each A-mode scan has 496 pixels with $3.8\mu m$ resolution. The system acquires the images at a given frame-rate (8.8 frames/second) and with a given bit depth (32-bits). The images, all centered on the macula, were taken from both eyes. OCT scans centered on the macula are widely used since clinicians employ this imaging modality to study this specific region of the eye fundus in the context of different pathologies.

Table 1 Results of the intersections correction process.

	Correction of crossings	**Correction of bifurcations**
Sensitivity (%)	82.75	99.54
Specificity (%)	99.56	76.28
Accuracy (%)	94.98	92.47
MCC (%)	87.28	82.26

Given the complexity of the manual segmentation of the entire vessel tree, we did not carry out a global analysis of the entire vasculature automatic segmentation process. Instead, specific tests of key steps of the methodology were performed to provide a more insightful idea of the robustness of the defined stages.

Intersections represent one of the most difficult structures of the vasculature. For that reason, we analyzed the **performance of the intersections correction process** to determine the extent to which the method is capable of correctly representing these complex vasculature regions. 87 crossings and 222 bifurcations were manually annotated by a specialist from within the image dataset. Then, we analyzed whether the method identified them correctly using the manual labeling as a reference. The metrics obtained are presented in Table 1, including the accuracy, sensitivity, specificity and the Matthews correlation coefficient (MCC). As we can see, satisfactory results were achieved. Figure 15 includes different examples of intersections that were correctly handled by the methodology. In particular, Figure 15 Row 1 includes four complex crossings, with vessels that are significantly close to each other, including a highly complicated case of a multiple crossing involving several vessels. Figure 15 Row 2 shows a heterogeneous set of bifurcations including a double chained intersection and another bifurcation with a close crossing that could interfere with the correct identification of this junction.

Another crucial stage is that of **vessel caliber estimation**. In order to measure the performance of our method in this respect, we constructed a test set with 220 random points from 24 segments , also randomly selected. Again, a specialist annotated the diameters of the selected points to use as a reference to test the performance of this automatic stage of the proposal. At each point, the corresponding error is calculated as:

$$Error = d_e - d_c \tag{10}$$

whereas the relative error is:

$$Relative\_Error = \frac{d_e - d_c}{d_e} \tag{11}$$

where d_e is the annotated diameter and d_c is the diameter resulting from the method. Table 2 presents the errors obtained by the caliber estimation process.

Fig. 15 3D visualization of intersections correctly managed. Row 1: examples of crossings. Row 2: examples of intersections.

Table 2 Errors obtained by the caliber estimation process.

	Error	**Relative error**
Global mean	0.1813	0.0438
Global standard deviation	0.3190	0.0754

Table 3 Results obtained for the vessel mapping and depth calculation stages of the methodology.

	Vessel mapping in OCT	**Depth calculation**
Correctly processed	1,168	1,433
Test set size	1,348	1,561
Success rate (%)	86.64	91.80

The next step is **vessel mapping in the OCT sections**. We conducted another experiment to quantitatively validate the vessel mapping process. A set of 1,348 mapped points randomly taken from the entire image dataset was selected for validation. In this case, a success is considered to be where a point is mapped by the method within the annotated projection zone. The results, shown in Table 3, indicate an accuracy of over 86%. Figure 16 shows four successful mapping examples including the corresponding projection zones in the OCT sections.

A further test was designed to validate the robustness of the **depth estimation**. An expert clinician segmented the vessels in the OCT images, constructing a set of 1,561 annotated vessel points that were randomly selected. The gold standard establishes that a success is considered to be when the location result falls inside the manual segmentation. As presented in Table 1,

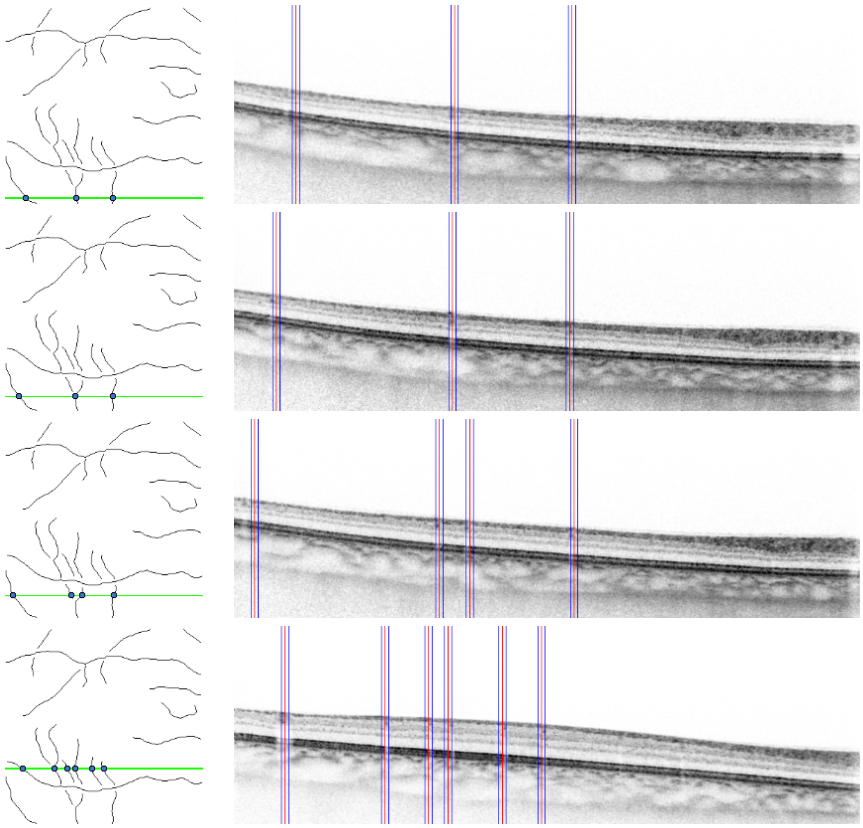

Fig. 16 Vessel mapping in the OCT sections. (a) Near-infrared reflectance retinography with the intersection of vessels at the band of an OCT section. (b) Identification of the projection zone of a mapped vessel point.

a success rate of 91.80% was obtained, demonstrating the robustness of the proposal. Figure 17 presents eight examples of correct vessel identifications inside the projection zones.

Figure 18 includes three examples of final 3D reconstructions. They illustrate the potential of the 3D extraction and reconstruction of the arteriovenous tree with respect to classical 2D segmentations for further analysis and diagnostic processes. In general terms, and in the opinion of the experts, the method offers correct and promising results, providing an innovative 3D vasculature view that constitutes a better representation of the real layout of the vessels than that given by classical 2D representations.

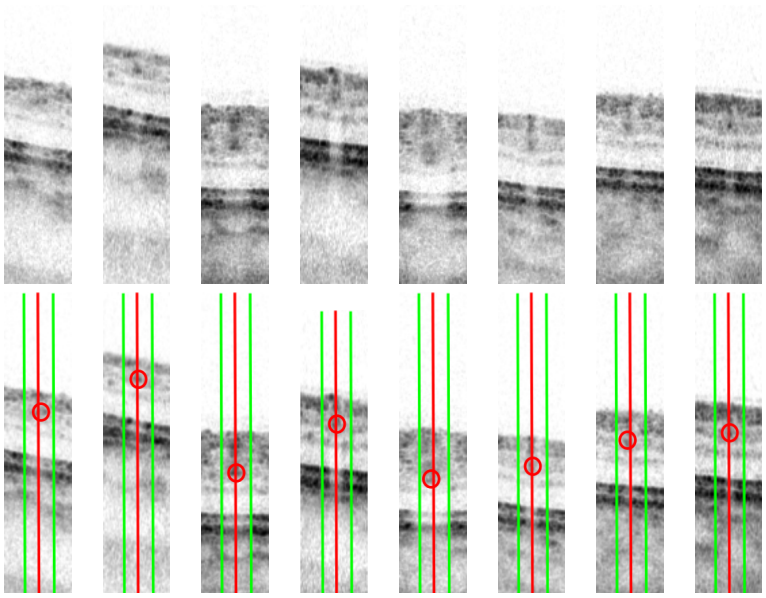

Fig. 17 Examples of correct vessel depth identifications. Row 1: vessels to be located. Row 2: obtained detections.

4 Discussion

The identification of the vasculature in the near-infrared reflectance retinography guarantees the use of a robust and proven methodology to identify the locations of the vessels, even in the case of the identification of small vessels, a typical situation in the macular region. This way, we only map the vascular profiles in the OCT sections and calculate their depth, using the spatial coordinates and their caliber. The support of the near-infrared reflectance retinography, provided directly by the capture machine in combination with the OCT sections, greatly facilitates this work, with only those areas in the sections that belong to real vessels being analyzed.

This methodology takes OCT images focused on macula as its input. The macular region includes the smallest and most tenuous vasculature of the retina, and for this reason we consider that the tests were carried out in one of the most complex scenarios available. In other areas the vessels are thicker and more visible, presenting a higher contrast that facilitates their detection.

The method was tested under a set of images that were captured from healthy individuals and patients presenting diabetic retinopathy or hypertension, proving the capability of the method to identify the vasculature under a large variability of conditions. These conditions may produce changes mainly in the vascular calibers (thickening, narrowing or appearance of small protuberances) or in the vascular structure (increased tortuosity or neovascularization). These changes do not alter the vessel visualization in the retinography as well as the shadow projection in the OCT sections. In addition, the three-

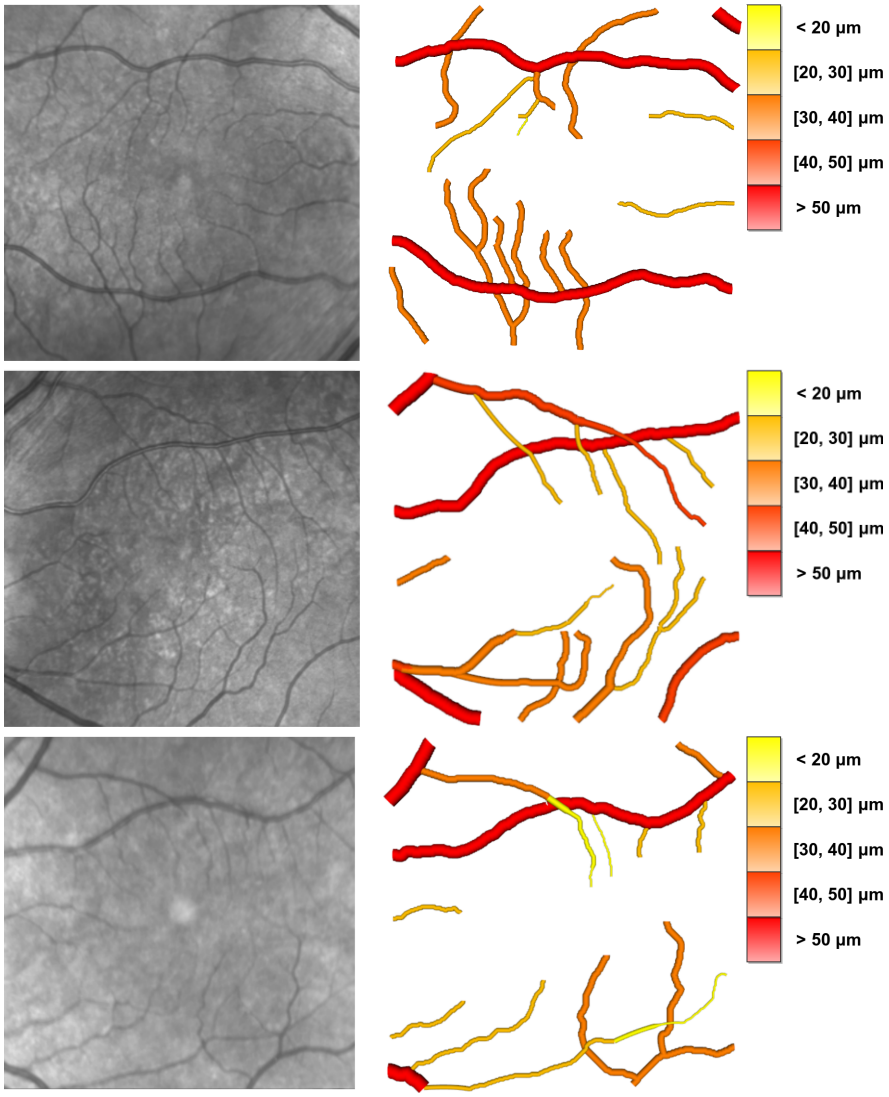

Fig. 18 Final 3D reconstructions of the vessel tree. 1^{st} column: original images. 2^{nd} column: final 3D reconstructions.

dimensional visualization of the real layout of the vasculature that this method provides facilitates the analysis and identification of these changes.

As no other complete 3D methods have been published to date we are unable to perform any kind of comparison with other proven approaches. Instead, we used the opinion of expert clinicians to identify the relevant stages of the method and test its performance, validating its accuracy as compared to manual annotations by the experts at key stages of the methodology.

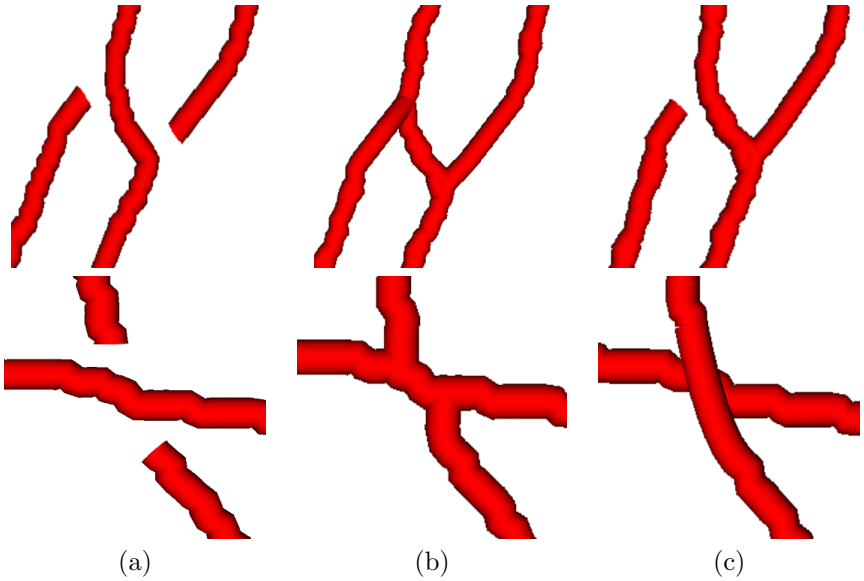

Fig. 19 Examples of intersections incorrectly managed. 1^{st} row, bifurcation. 2^{nd} row, crossing. (a) Vessel detection before intersection correction. (b) Corrected vasculature. (c) Desired result.

Most of the errors came from complex intersections more often than not involving more than two segments. Examples of this can be found in Figure 19, where two intersections that were not correctly included are presented. The columns represent the original vessel detection, the final results of the method and the desired results, respectively. In the case of Figure 19 Row 1, as we can see from the desired result, the analyzed region belongs to a junction of 3 different vessels. Two of them constitute an intersection but the third belongs to the end of a vessel, with no real final connection. However, given the proximity of this end point, the method interprets that another intersection exists. Figure 19 Row 2 shows a particular case where the method interprets two different bifurcations instead of a crossing.

Normally, methodologies for retinal vasculature identification omit tiny vessels in the image. In the case of our method, we consider it important to mention the high rate of detection of vessels appearing in the macular region, a region of the eye fundus where vessels are smaller than in the rest of the retina. The errors in caliber estimation are presented in Table 2. Given the complexity of the images, with a significant noise level and blurred vessel contours, it is often highly complicated to exactly detect the limits. For this reason, a relative error rate in the estimation of vasculature calibers of about only 4% can be considered to be more than acceptable.

Figure 20 includes two incorrect mapping examples. Most of the failures tend to occur when the detected vessel is elongated in parallel to the band of the OCT sections. In these cases, the method is not capable of correctly

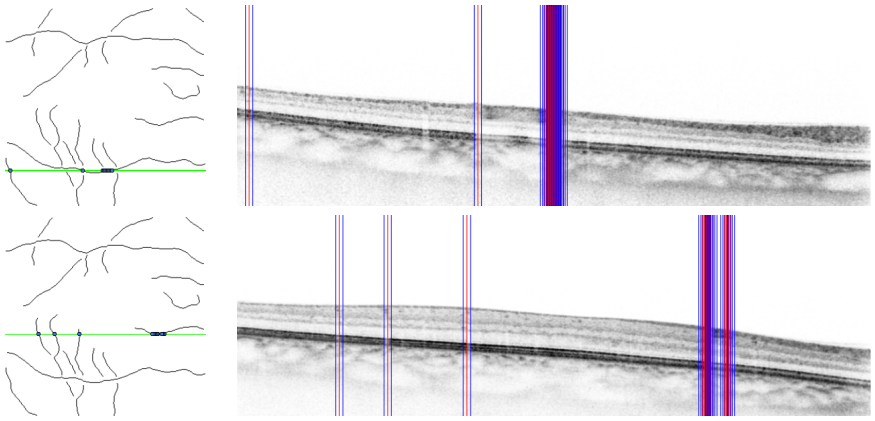

Fig. 20 Examples of incorrect vessel mappings in the corresponding OCT sections. (a) Near-infrared reflectance retinography with the intersection of vessels at the band of a OCT section. (b) Identification of the projection zone of a mapped vessel point.

matching the exact point of the intersection. This situation could be minimized through the use of higher resolutions, which could help to discriminate the exact intersection points. Alternatively, OCT sections in the perpendicular direction or radial directions, as provided by some capture machines, could also help to minimize these errors.

We also present a number of incorrect detections in the vessel location phase, as shown in Figure 21. In this case, although the method finds the darkest spot between the ILM and RPE layers, it belongs to noisy artifacts or overlapping vessels, not to the target vessel. Incorrect detections are on the whole mainly due to: (1) noisy artifacts or vessels that are too close to and appear in the same region of the OCT section as the target vessel position; (2) alterations of a particular layer producing dark regions that can be confused with a vessel; and (3) the impossibility of detecting the dark spot of a vessel. In the latter case, this is because vessels are at times located in parallel to the OCT section, and thus do not produce the typical dark spot that identifies a vessel.

5 Conclusions

This work presents a new fully automatic methodology to obtain the 3D segmentation and reconstruction of the retinal arteriovenous tree using OCT images. A 3D representation offers a more complete set of information for the analysis of the retinal microcirculation, in contrast to the 2D visualizations of classical retinographies, enabling more accurate analysis and diagnosis in different clinical procedures. Vessel tree analysis is crucial for the early diagnosis of several relevant diseases such as nicking (AV nicking) or retinal vascular

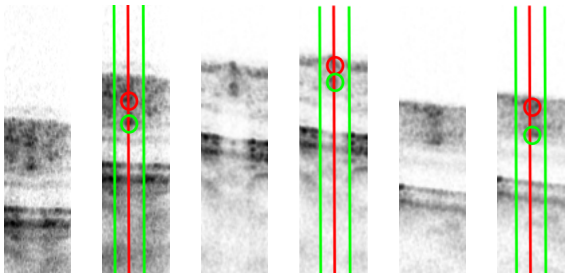

Fig. 21 Examples of wrong vessel depth identifications. 1^{st} column, vessels to locate. 2^{nd} column, results: red circle, the obtained vessel location: green circle, real vessel location.

tortuosity. AV nicking is the situation where a small arteriole is swollen or dilated and crosses over a vein compressing it and is a highly relevant indicator in prevalent conditions that alter the caliber of vessels. For its part, retinal vascular tortuosity indicates the degree of elongation or bending of the retinal vasculature. Both are signs of hypertension, arteriosclerosis or other vascular conditions and a 3D representation of the vessels can lead to more accurate identifications and measurements of both indicators.

The proposed method covers the entire automatic segmentation process: initial 2D vasculature identification, caliber estimation and mapping in the OCT images to calculate the depth coordinates. Finally, the method uses the resulting (x, y, z) vasculature coordinate set combined with their calibers d to reconstruct the entire vessel tree. The proposed approach was validated with 21 patient scans summing an image dataset of 991 OCT sections with their corresponding near-infrared reflectance retinographies. Key stages of the methodology were tested, providing coherent and promising results.

In future works, we plan to analyze and improve the different stages to achieve higher success rates. Automatic artery and vein classification is also planned for inclusion, adding valuable information to retinal microcirculation analysis in any diagnostic process. Images with perpendicular or radial sections will also be tested with the aiming of reducing the limitation of the method in its application in the same direction, in all cases. In addition, further validations will be made in the other areas of the retina, to confirm the accuracy of the proposal with bigger and cleaner vessels. Despite the difficulties, we will also inspect new methods to extract the vascular structure directly in the OCT sections, using only these images for the whole 3D reconstruction process and thereby avoiding the multimodality dependence of near-infrared reflectance retinography. The identification of the three-dimensional structure or the retinal vasculature could serve as input in posterior clinical studies that may involve the calculation and analysis of different measurements, as tortuosity or the arterio-venular-ratio. These measurements were typically calculated in two dimensions, mainly in the analysis of classical retinographies. Extension to three dimensions could be achieved using the real layout of the vasculature that may lead to more precise analysis and diagnosis.

Acknowledgements This work is supported by the Instituto de Salud Carlos III, Government of Spain and FEDER funds of the European Union through the PI14/02161 and the DTS15/00153 research projects and by the Ministerio de Economía y Competitividad, Government of Spain through the DPI2015-69948-R research project. Also, this work has received financial support from the European Union (European Regional Development Fund - ERDF) and the Xunta de Galicia, Centro singular de investigación de Galicia accreditation 2016-2019, Ref. ED431G/01; and Grupos de Referencia Competitiva, Ref. ED431C 2016-047.

References

1. Alonso-Montes, C., Vilarino, D.L., Penedo, M.G.: Automated localization of the optic disc, fovea, and retinal blood vessels from digital colour fundus images. International Workshop on Cellular Neural Networks and Their Applications pp. 61–64 (2005)
2. Calvo, D., Ortega, M., Penedo, M.G., Rouco, J.: Automatic detection and characterisation of retinal vessel tree bifurcations and crossovers in eye fundus images. Computer Methods and Programs in Biomedicine **103**, 28–38 (2011)
3. Chakraborti, T., Jha, D.K., Chowdhury, A.S., Jiang, X.Y.: A self-adaptive matched filter for retinal blood vessel detection. Machine Vision and Applications **26**(1), 55–68 (2015)
4. Chen, X., Niemeijer, M., Zhang, L., Kyungmoo, L., Abramoff, M. D., and Sonka, M.: Three-dimensional segmentation of fluid-associated abnormalities in retinal OCT: probability constrained graph-search-graph-cut. IEEE Trans. Medical Imaging **31**(8), 1521–1531 (2012)
5. Cheng, E.K., Du, L., Wu, Y., Zhu, Y.J., Megalooikonomou, V., Ling, H.B.: Discriminative vessel segmentation in retinal images by fusing context-aware hybrid features. Machine Vision and Applications **25**(7), 1779–1792 (2014)
6. de Carlo, Talisa E and Romano, Andre and Waheed, Nadia K and Duker, Jay S: A review of optical coherence tomography angiography (OCTA). International Journal of Retina and Vitreous **1**(1), 5 (2015)
7. De Jong, F.J., Ikram, M.K., Witteman, J.C., Hofman, A., De Jong, P.T., and Breteler, M.M.: Retinal vessel diameters and the role of inflammation in cerebrovascular disease. Annals of Neurology Journal **61**(5), 491–495 (2007)
8. Dhar, R., Gupta, R., Baishnab, K.L.: An analysis of canny and laplacian of gaussian image filters in regard to evaluating retinal image. Int. Conference on Green Computing Communication and Electrical Engineering **31**(8), 1–6 (2014)
9. Dougherty, E.: Mathematical Morphology in Image Processing (1993)
10. Fathi, A., Naghsh, N., Reza, A.: Blood vessels segmentation in retina: Preliminary assessment of the mathematical morphology and of the wavelet transform techniques. Biomedical Signal Processing and Control Journal **8**(1), 71–80 (2013)
11. Frangi, A.F., Niessen, W.J., Vincken, K.L., Viergever, M.A.: Multiscale vessel enhancement filtering. Proc. of the Medical Image Computing and Computer-Assisted Interventation (MICCAI) pp. 130–137 (1998)
12. Fraz, M.M., Remagnino, P., Hoppe, A. Uyyanonvara, B., Rudnicka, A.R., Owen, C.G., Barman, S.A.: Blood vessel segmentation methodologies in retinal images - A survey. Computer Methods and Programs in Biomedicine **108**(1), 407–433 (2012)
13. Guimaraes, P., Rodrigues, P., Bernardes, R., Serranho, P.: 3D blood vessels segmentation from optical coherence tomography. Acta Ophthalmologica (2012)
14. Imani, E., Javidi, M., Pourreza, H.R.: Improvement of retinal blood vessel detection using morphological component analysis. Computer Methods and Programs in Biomedicine **118**(3), 263–279 (2015)
15. Jiang, P., Dou, Q.S., Hu, X.Y.: A supervised method for retinal image vessel segmentation by embedded learning and classification. Journal of Intelligent and Fuzzy Systems **29**(5), 2305–2315 (2015)
16. Klein, R., Klein, B., Moss, S., Wong, T., and Sharrett, A.: Retinal vascular caliber in persons with type 2 diabetes: the Wisconsin Epidemiological Study of Diabetic Retinopathy: XX. Ophthalmology Journal **113**(9), 1488–1498 (2006)

17. Kovacs, G., Hajdu, A.: A self-calibrating approach for the segmentation of retinal vessels by template matching and contour reconstruction. Medical Image Analysis **29**(4), 24–46 (2016)
18. Lazar, I., Hajdu, A.: Segmentation of retinal vessels by means of directional response vector similarity and region growing. Computers in Biology and Medicine **66**(1), 209–221 (2015)
19. Li, Q.L., Feng, B.W., Xie, L.P., Liang, P., Zhang, H.S., Wang, T.F.: A Cross-Modality Learning Approach for Vessel Segmentation in Retinal Images. IEEE Transactions on Medical Imaging **35**(1), 109–118 (2016)
20. López, A., Lloret, D., Serrat, J., Villanueva, J.J.: Multilocal creaseness based on the level set extrinsic curvature. Computer Vision and Image Understanding **77**, 111–144 (2000)
21. Mendonça, A.M., Campilho, A.: Segmentation of retinal blood vessels by combining the detection of centerlines and morphological reconstruction. IEEE Trans. Med. Imaging **25**(9), 1200–1213 (2006)
22. Nayak, C.: Retinal blood vessel segmentation algorithm for diabetic retinopathy using wavelet: a survey. Int. J. on Recent and Innovation Trends in Comp. and Comm. **3**(3), 927–930 (2013)
23. Nguyen, T. T., Wang, J. J., Sharrett, A. R., Islam, F. A., Klein, R., Klein, B. E., Cotch, M. F., and Wong, T. Y.: Relationship of retinal vascular caliber with diabetes and retinopathy: The multi-ethnic study of atherosclerosis (MESA). Diabetes Care Journal **31**(3), 544–549 (2007)
24. Niemeijer, M., Garvin, M.K., van Ginneken, B., Sonka, M., Abrámoff, M.D.: Vessel segmentation in 3D spectral OCT scans of the retina. SPIE 2008 proceedings (2008)
25. Ortega, M., Penedo, M.G., Rouco, J., Barreira, N., Carreira, M.J.: Personal verification based on extraction and characterisation of retinal feature points. Journal of Visual Languages and Computing **20**(2), 80–90 (2009)
26. Patton, N., Aslam, T., MacGillivray, T., Pattie, A., Deary, I. J., and Dhillon, B.: Retinal vascular image analysis as a potential screening tool for cerebrovascular disease: a rationale based on homology between cerebral and retinal microvasculatures. Annals of Neurology Journal **206**(4), 319–348 (2005)
27. Pilch, M., Wenner, Y., Strohmayr, E., Preising, M., et al.: Automated segmentation of retinal blood vessels in spectral domain optical coherence tomography scans. Biomedical Optic Express **3**(7), 1478–1491 (2012)
28. Sinthanayothin, C., Boyce, J.F., Cook, H.L., and Williamson, T.H.: Automated localization of the optic disc, fovea, and retinal blood vessels from digital colour fundus images. British Journal of Ophthalmology **83**(3), 902–911 (1999)
29. Smith, W., Wang, J. J., Wong, T. Y., Rochtchina, E., Klein, R., Leeder, S. R., and Mitchell, P.: Retinal arteriolar narrowing is associated with 5-year incident severe hypertension: The Blue Mountains eye study. Hypertension Journal **44**(4), 442–447 (2004)
30. Soares, J., Leandro, J., Cesar, R., Jelinek, H., Cree, M.: Retinal vessel segmentation using the 2-d gabor wavelet and supervised classification. IEEE Transactions on Medical Imaging **25**(9), 1214–1222 (2006)
31. Staal, J., Abramoff, M.D., Niemeijer, M., Viergever, M.A., van Ginneken, B.: Ridge based vessel segmentation in color images of the retina. IEEE Transactions on Medical Imaging **23**(4), 501–509 (2004)
32. Sun, C., Liew, G., Wang, J.J., Mitchell, P., Saw, S.M., Aung, T., Tai, E.S., and Wong, T.Y.: Retinal vascular caliber, blood pressure, and cardiovascular risk factors in an Asian Population: The Singapore Malay eye study. Investigative Opthalmology and Visual Science Journal **49**(5), 1784–1790 (2008)
33. Vega, R., Sanchez-Ante, G., Falcon-Morales, L.E., Sossa, H., Guevara, E.: Retinal vessel extraction using Lattice Neural Networks with dendritic processing. Computers in Biology and Medicine **58**(1), 20–30 (2015)
34. Wink, O., Niessen, W.J., and Viergever, M.A.: Adaptive local thresholding by verification-based multithreshold probing with application to vessel detection in retinal images. IEEE Transactions on Medical Imaging **23**(1), 130–133 (2004)
35. Wong, T.Y.: Quantitative retinal venular caliber and risk of cardiovascular disease in older persons. Archives of Internal Medicine Journal **166**(21), 2388–2394 (2006)

36. Wu, J., Gerendas, B., Waldstein, S., Langs, G., et al.: Stable registration of pathological 3D-OCT scans using retinal vessels. Ophthalmic Medical Image Analysis, 2014. Proceedings of (2014)
37. Xiaolin, S., Zhenhua, C., Chuang, M., Yonghang, J., Duan, Z. Y., Wang, L. G., and Chang, S.H.: Retinal vessel tracking using bilateral filter based on canny method. International Conference on Audio, Language and Image Processing pp. 1678–1682 (2010)
38. Xiaoyi, J., Mojon, D.: Adaptive local thresholding by verification-based multithreshold probing with application to vessel detection in retinal images. IEEE Transactions on Pattern Analysis and Machine Intelligence **25**(1), 131–137 (2003)
39. Xu, J., Tolliver, D.A., Ishikawa, H., Wollstein, G., Schuman, J.S.: 3D OCT retinal vessel segmentation based on boosting learning. Medical Image Analysis **25**(11), 179–182 (2009)
40. Xu, X., Niemeijer, M., Song, Q., Garvin, M.K., Reinhardt, J.M., Abramoff, M.D.: Retinal vessel width measurements based on a graph-theoretic method. IEEE International Symposium on Biomedical Imaging: From Nano to Macro pp. 641–644 (2011)
41. Yin, B.J., Li, H.T., Sheng, B., Hou, X.H., Chen, Y., Wu, W., Li, P., Shen, R.M., Bao, Y.Q., Jia, W.P.: Vessel extraction from non-fluorescein fundus images using orientation-aware detector. Medical Image Analysis **26**(1), 232–242 (2015)
42. Yong, Y., Yuan, Z., Shuying, H., Nini, R., Zhijun, F., and Jucheng, Y.: Effective combined algorithms for retinal blood vessels extraction. Advances in Information Sciences and Service Sciences Journal **4**(3), 263–269 (2012)
43. Zhang, Y., Hsu, W., Lee, M.L.: Segmentation of retinal blood vessels by combining the detection of centerlines and morphological reconstruction. Journal of Signal Processing Systems **55**(1), 103–112 (2008)

Joaquim de Moura received his degree in Computer Engineering in 2014 from the University of A Coruña (Spain). In 2016, he received his M.Sc degree in Computer Engineering from the same university. He is currently pursuing his Ph.D. degree in Computer Science in a collaborative project between ophthalmology centers in Galicia and the University of A Coruña. His research interests include computer vision, machine learning algorithms and analysis and medical imaging processing of various kinds.

Jorge Novo received his M.Sc. and Ph.D. degrees (cum Laude) in Computer Science from the University of A Coruña in 2007 and 2012, respectively. He has also worked, as a visiting researcher, with CMR images in the detection of landmark points at Imperial College London and as a post-doctoral research fellow at the INEB and INESC-TEC research institutes in the development of CAD systems for lung cancer diagnosis with chest CT images. His main research interests lie in the fields of computer vision, pattern recognition and biomedical image processing.

Pablo Charlón received his M.Sc. degree from the University of Santiago de Compostela, Spain in 2011, specializing in the field of Vision Science Research. Currently he is working as a Clinical Optometrist at the Victoria de Rojas Ophthalmological Institute in A Coruña, Spain. He is also the president of the Galician Society of Clinical Optometry. His research interests lie in the field of ophthalmology, where he has published a number of research articles on OCT imaging.

Noelia Barreira received her Master's and Ph.D degrees in Computer Science from the University of A Coruña (Spain) in 2003 and 2009, respectively. She is currently an Associate Professor in the Computer Science Department at the University of A Coruña. Her research interests lie in the fields of computer vision, pattern recognition, biomedical image processing and machine learning.

Marcos Ortega received his M.Sc. degree in Computer Science in 2004 and his Ph.D. degree cum Laude in 2009. He also worked on face biometrics studying the face evolution due to aging effects as a visiting researcher in the University of Sassari and methods for age estimation under different facial expression conditions as a visiting postdoctoral fellow in the University of Amsterdam. He is currently an Associate Professor in the Department of Computer Science at the University of A Coruña. His research areas of interest are medical image analysis, computer vision, biometrics and human behaviour analysis.